
This is an electronic reprint of the original article.
This reprint may differ from the original in pagination and typographic detail.

Chen, Min; Avarmaa, Katri; Taskinen, Pekka; Michallik, Radoslaw; Jokilaakso, Ari
Investigation on the Matte/Slag/Spinel/Gas Equilibria in the Cu-Fe-O-S-SiO₂-(CaO, Al₂O₃) system at 1250 °C and pSO₂ of 0.25 atm

Published in:
Mineral Processing and Extractive Metallurgy Review

DOI:
[10.1080/08827508.2022.2047966](https://doi.org/10.1080/08827508.2022.2047966)

Published: 01/01/2023

Document Version
Publisher's PDF, also known as Version of record

Published under the following license:
CC BY-NC-ND

Please cite the original version:
Chen, M., Avarmaa, K., Taskinen, P., Michallik, R., & Jokilaakso, A. (2023). Investigation on the Matte/Slag/Spinel/Gas Equilibria in the Cu-Fe-O-S-SiO₂-(CaO, Al₂O₃) system at 1250 °C and pSO₂ of 0.25 atm. *Mineral Processing and Extractive Metallurgy Review*, 44(4), 313-324.
<https://doi.org/10.1080/08827508.2022.2047966>

This material is protected by copyright and other intellectual property rights, and duplication or sale of all or part of any of the repository collections is not permitted, except that material may be duplicated by you for your research use or educational purposes in electronic or print form. You must obtain permission for any other use. Electronic or print copies may not be offered, whether for sale or otherwise to anyone who is not an authorised user.

Mineral Processing and Extractive Metallurgy Review

An International Journal

ISSN: (Print) (Online) Journal homepage: <https://www.tandfonline.com/loi/gmpr20>

Investigation on the Matte/Slag/Spinel/Gas Equilibria in the Cu-Fe-O-S-SiO₂-(CaO, Al₂O₃) system at 1250 °C and *p*SO₂ of 0.25 atm

Min Chen, Katri Avarmaa, Pekka Taskinen, Radoslaw Michallik & Ari Jokilaakso

To cite this article: Min Chen, Katri Avarmaa, Pekka Taskinen, Radoslaw Michallik & Ari Jokilaakso (2023) Investigation on the Matte/Slag/Spinel/Gas Equilibria in the Cu-Fe-O-S-SiO₂-(CaO, Al₂O₃) system at 1250 °C and *p*SO₂ of 0.25 atm, Mineral Processing and Extractive Metallurgy Review, 44:4, 313-324, DOI: [10.1080/08827508.2022.2047966](https://doi.org/10.1080/08827508.2022.2047966)

To link to this article: <https://doi.org/10.1080/08827508.2022.2047966>



© 2022 The Author(s). Published with license by Taylor & Francis Group, LLC.



Published online: 10 Mar 2022.



Submit your article to this journal [↗](#)



Article views: 783



View related articles [↗](#)



View Crossmark data [↗](#)



Citing articles: 3 View citing articles [↗](#)

Investigation on the Matte/Slag/Spinel/Gas Equilibria in the Cu-Fe-O-S-SiO₂-(CaO, Al₂O₃) system at 1250 °C and *p*SO₂ of 0.25 atm

Min Chen , Katri Avarmaa ^{a,b}, Pekka Taskinen , Radoslaw Michallik^c and Ari Jokilaakso 

^aDepartment of Chemical and Metallurgical Engineering, School of Chemical Engineering, Aalto University, Aalto, Finland; ^bDepartment of Mechanical and Product Design Engineering, Swinburne University of Technology, Melbourne, Victoria, Australia; ^cGeological Survey of Finland, Espoo, Finland

ABSTRACT

The equilibrium-phase relations between copper mattes and spinel-saturated iron silicate slags were investigated at 1250°C and *p*SO₂ of 0.25 atm. The experiments were conducted in synthesized spinel crucibles (Fe₃O₄) in controlled CO-CO₂-SO₂-Ar gas mixtures using a high-temperature isothermal equilibration/quenching technique. The equilibrium-phase compositions were characterized using an electron probe X-ray microanalyzer. The compositions of matte and slag were displayed as a function of matte grade or oxygen partial pressure. The present results obtained at spinel saturation in the matte-slag equilibrium system were compared with observations in the literature. This study improves the experimental thermodynamic data on the matte-slag-spinel-gas equilibria systems.

KEYWORDS

Phase equilibria; copper smelting; spinel; slag chemistry; thermodynamics

1. Introduction

The Cu-Fe-S-O-SiO₂-(CaO-MgO-Al₂O₃) system plays an essential role in the pyrometallurgical processing of copper sulfide ores forming the basis of the fayalite slags and the iron sulfide-based mattes (Djordjevic et al. 2014; Li and Rankin 1994; Nikolic, Hayes and Jak 2009). Accurate information of this system in the matte-slag-gas phase equilibria provides guidance to improve the industrial operation and performance of the copper smelters, as well as to develop the databases used by different simulation and computational modeling programs.

Much work has been done for the matte-slag-gas equilibria at silica saturation; however, only limited data exist for the systems at iron spinel saturation, mainly due to the difficulties of conducting experiments with the aggressive slags formed during the annealing and when aiming to achieve an appropriate quenching. The iron spinel is a common phase formed in the copper smelting processes (Chen et al. 2015; Hidayat et al. 2020; Shishin et al. 2016; Sun et al. 2020f; Wan et al. 2021; Wang et al. 2019); therefore, to deepen our understanding of the copper matte smelting processes, it is important to determine the phase relations of the spinel saturated matte-slag-gas equilibrium systems.

Hidayat et al. (2016, 2018, 2020) investigated the matte/slag/spinel/gas equilibria in the Cu-Fe-Si-S-O system at 1200–1250°C and *p*SO₂ of 0.25 atm. It was reported that the concentration of sulfur, “FeO,” and copper in slag increased with increasing temperature at a given matte grade. Chen et al. (2019) and Sun et al. (2020a, 2020b) studied the effects of MgO and CaO on the matte/slag/spinel/gas equilibria in the Cu-Fe-Si-S-O system at *p*SO₂ of 0.3 and 0.6 atm with fixed matte grade of 72 wt% Cu and in temperature range of 1180–1250°C. It was indicated that the presence of MgO and CaO has a similar increasing impact on

the liquidus temperature of the iron silicate slags at a fixed SO₂ partial pressure. However, MgO exhibited a stronger impact than CaO at 1250°C. Moreover, they (Sun et al. 2020c, 2020d, 2020e, 2020f, 2020g) also equilibrated blister copper/white metal and spinel saturated FeO_x-SiO₂/FeO_x-SiO₂-CaO slags under conditions of *p*SO₂ = 0.4 atm, *p*O₂ = 10⁻⁶ to 10⁻⁵ atm, and T = 1250–1300°C, related to the blister copper making and copper converting processes. Sineva et al. (2020), Sineva et al. (2021a)) determined the effects of SO₂ partial pressure, and concentrations of Al₂O₃, CaO, and MgO on the matte/slag/spinel/gas equilibria at 1200°C. They found the dissolved copper in slags decreased with increasing *p*SO₂ at a constant matte grade. The concentrations of iron, sulfur, and chemically dissolved copper in slags decreased with increasing Al₂O₃, MgO, and CaO concentrations. A detailed literature review on the available studies for matte-slag-gas equilibria at silica/MgO saturation can be found in our previous studies (Chen et al. 2020a, 2020b).

In summary, the matte/slag/spinel/gas equilibria have not been studied extensively and the effects of Al₂O₃ and CaO on this equilibrium system have not been investigated in copper matte smelting conditions. Therefore, this study investigated the phase equilibrium relations between copper mattes and iron spinel-saturated iron silicate slags (FeO_x-SiO₂, FeO_x-SiO₂-Al₂O₃, and FeO_x-SiO₂-CaO) at 1250°C and *p*SO₂ of 0.25 atm. The results presented enrich the experimental thermodynamic data for the matte-slag-spinel-gas equilibrium system and subsequently provide insights for improving the copper smelting processes.

2. Experimental

High purity powders of Cu₂S (Alfa Aesar, –200 mesh, 99.5 wt%) and FeS (Alfa Aesar, –100 mesh, 99.9 wt%) were used to synthe-

size the copper matte mixtures. The slag mixtures were prepared using Fe_2O_3 (Alfa Aesar, 99.998 wt%), SiO_2 (Alfa Aesar, -40 mesh, 99.995 wt%), Al_2O_3 (Sigma-Aldrich, 99.99 wt%), and CaO (Sigma-Aldrich, 99.90 wt%) with initial slag compositions of $\text{Fe}_2\text{O}_3/\text{SiO}_2 = 80/20$, $\text{Fe}_2\text{O}_3/\text{SiO}_2/\text{Al}_2\text{O}_3 = 62/28/10$, and $\text{Fe}_2\text{O}_3/\text{SiO}_2/\text{CaO} = 62/28/10$, respectively. Additionally, trace metals of Ag, Ni, Co, and Sn were included in the system, but their distribution behaviors will be disclosed in a subsequent paper. Approximately 0.2 g of copper matte mixture and equal amount of slag mixture were pressed into a pellet using a hydraulic press for each experiment. Gas mixtures of CO (99.99 vol%), CO_2 (99.999 vol%), SO_2 (99.99 vol%) and Ar (99.999 vol%), all from Linde-AGA Finland, were used to control the gas atmosphere in the reaction tube. DFC26 digital mass-flow controllers (Aalborg, USA) were used to regulate the flow rates of all gases. The partial pressures of O_2 and S_2 for different target matte grades were calculated using MTDATA thermodynamic software (Davies et al. 2002; Gisby et al. 2017) with its SGTE pure substance database, shown in Table 1. All sample pellets were equilibrated at high temperature in iron spinel (Fe_3O_4) crucibles that were prepared by oxidizing the folded iron foil (thickness 0.25 mm, 99.5 wt%, Sigma Aldrich & Merck) at 1200°C and $p\text{O}_2$ of 10^{-8} atm for 4 h. To verify the oxidized iron foil composition, one crucible prepared was crushed into powders and analyzed by X-ray diffraction (XRD, PANalytical X'Pert Powder XRD (alpha-1), The Netherlands) using Cu K α radiation (40 kV, 40 mA). The XRD pattern of the synthesized spinel crucible, shown in Figure 1, indicates that metallic iron was fully oxidized to Fe_3O_4 .

The high-temperature isothermal equilibration experiments were carried out in a vertical alumina tube furnace (Lenton PTF 15/45/450, UK) employing SiC heating elements (Kanthal, UK). The temperature of the sample was monitored with a calibrated S-type, Pt/90 wt% Pt-10 wt% Rh thermocouple (Johnson-Matthey Noble Metals, UK) (Avarmaa et al. 2018b). The experiments followed the routine of high-temperature isothermal equilibration in controlled gas atmosphere, rapid quenching in ice-water mixture, and the phase characterization by EPMA (electron probe microanalyzer). Detailed experimental procedures utilized in this study are reported in previous publications (Avarmaa, Johto and Taskinen 2016; Avarmaa et al. 2022; Chen et al. 2021a, 2021b; Sukhomlinov et al. 2019b, 2020).

To determine the time needed to reach the equilibrium, time-series experiments were conducted by annealing matte and FeO_x - SiO_2 slag at 1250°C , $p\text{SO}_2 = 0.25$ atm, $p\text{O}_2 = 10^{-7.75}$ atm, and $p\text{S}_2 = 10^{-2.91}$ atm for 2, 4, and 6 hours. The equilibration time was determined based on the stabilization of the concentrations

Table 1. The calculated gas flow rates for different target $p\text{O}_2$ and $p\text{S}_2$ at 1250°C and $p\text{SO}_2$ of 0.25 atm.

Log[$p\text{O}_2$, atm]	Log[$p\text{S}_2$, atm]	Gas flow rates (mL/min)			
		SO_2	CO	CO_2	Ar
-7.50	-3.41	100.0	4.8	98.6	200.0
-7.62	-3.17	100.0	5.9	96.8	200.0
-7.75	-2.91	100.0	7.5	94.1	200.0
-7.84	-2.73	100.0	9.0	91.0	200.0
-7.90	-2.62	100.0	10.5	91.5	200.0

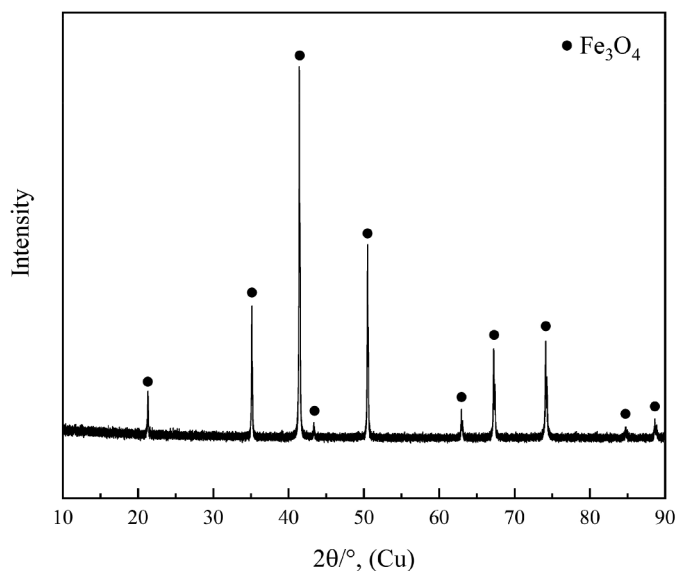


Figure 1. XRD pattern of the oxidized iron foil used as the primary phase, crucible material in the experiments.

of Cu, Fe, and S in matte as well as the concentrations of Cu, “FeO,” and SiO_2 in the slag measured by EDS. The results are presented in Figure 2 and it can be seen that the sample reached equilibrium in 4 hours; therefore, all samples were equilibrated under the experimental conditions for 4 hours.

The quenched samples were dried and mounted in epoxy resin. The samples were then ground and polished using a wet metallographic method. The polished cross sections were coated by carbon using a carbon vacuum evaporator (JEOL IB-29510VET). The microstructures and the major compositions of samples were pre-examined by a scanning electron microscope (SEM, Tescan MIRA 3, Brno, Czech Republic) equipped with an UltraDry Silicon Drift Energy Dispersive X-ray Spectrometer (EDS, Thermo Fisher Scientific, Waltham, MA, USA).

The chemical compositions of matte, slag, and spinel phases were characterized with a Cameca SX100 Electron Microprobe (Cameca SAS, Genevilliers, France) using the Wavelength Dispersive Spectrometers (WDS). The EPMA analysis was carried out at an acceleration voltage of 20 kV, beam current of 60 nA, and a probe diameter of 20 μm . The PAP on-line correction procedure (Pouchou and Pichoir 1986) fitted with the EPMA was applied for raw data processing. Standard materials of obsidian for O K α , quartz (SiO_2) for Si K α , metal Cu for Cu K α , almandine ($\text{Fe}_3\text{Al}_2(\text{SiO}_4)_3$) for Al K α , diopside ($\text{MgCaSi}_2\text{O}_6$) for Ca K α , and chalcopyrite (CuFeS_2) for Fe K α and S K α were used for calibrating the results. Table 2 shows the composition of obsidian used in EPMA analyses. Compared with hematite, using obsidian for oxygen measurement yields a better matrix correction for the light element oxygen due to the nature of the slags being glassy as well as the average electron density of both materials (slag and standard). At least 24 individual points were selected from the well-quenched areas of each phase, *i.e.* the matte, slag, and spinel phases, for calculating the average concentrations and their standard deviations.

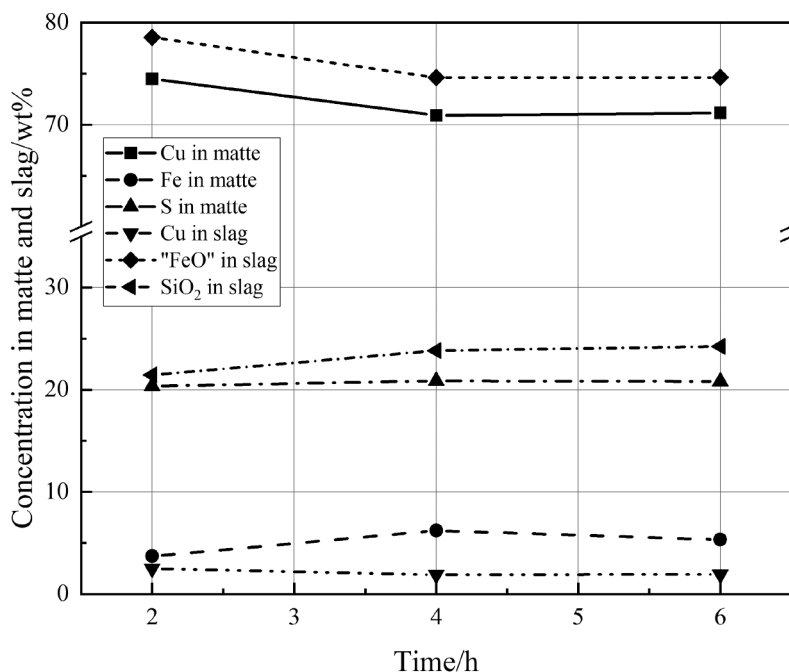


Figure 2. Concentrations of Cu, Fe, and S in matte as well as the concentrations of Cu, "FeO," and SiO₂ in slag as a function of equilibration time.

Table 2. Elemental composition of obsidian for oxygen measurement in EPMA analyses.

Element	H	O	F	Na	Mg	Al	Si	Cl	K	Ca	Ti	Mn	Fe	Sum
Concentration/wt%	0.09	48.63	0.07	3.01	0.04	6.94	34.56	0.36	4.18	0.54	0.06	0.05	1.34	99.87

3. Results and discussion

Figure 3 shows the typical microstructures of samples obtained at different conditions. The matte/slag/spinel/gas equilibria were confirmed in all samples. The amount of discrete spinel crystals in slags decreased with decreasing the prevailing oxygen partial pressure. Copper matte is difficult to be quenched into fully homogenized phase (Hidayat et al. 2018), and also in this study, copper-rich veins were found in the matte phase due to insufficient quenching rate. More copper-rich veins were observed in mattes with lower matte grades. The compositions of matte and liquid slag with standard deviations ($\pm 1\sigma$) measured by EPMA are shown in Table 3.

3.1 Matte composition

Figure 4 shows the concentrations of copper, iron, sulfur, and oxygen in matte as a function of oxygen partial pressure or matte grade. Data from literature (Chen et al. 2019; Hidayat et al. 2018, 2016, 2020; Sineva et al. 2020, 2021a) were also plotted in the figures for comparison.

3.1.1 Copper in matte vs $\text{Log}_{10}[pO_2, \text{atm}]$

Figure 4(a) and (b) indicates that the concentration of copper in matte equilibrated with all types of slags increased with increasing prevailing oxygen partial pressure since more iron was oxidized to the slag phase. Similar increasing trends were observed in the literature (Abdeyazdan et al. 2020a, 2020b; Chen et al. 2019; Fallah-Mehrjardi, Hayes and Jak 2018a; Fallah-Mehrjardi et al. 2017a, 2017b, 2018b; Hidayat et al. 2018, 2016,

2020; Roghani, Takeda and Itagaki 2000; Sineva et al. 2020, 2021a) and in our previous studies with silica saturation in slags (Avarmaa et al. 2015; Chen et al. 2020b, 2020c).

The addition of Al₂O₃ increased the copper concentration in matte at a fixed oxygen partial pressure, whereas the effect of CaO on matte grade at a given pO_2 was not evident. It has been reported previously that CaO has a stronger impact than Al₂O₃ on decreasing the activity of FeO in slag (Sukhomlinov et al. 2019a; Yazawa 1974), leading to a higher copper concentration in matte. Sineva et al. (2020) observed only minor effects of Al₂O₃, CaO, and MgO on the copper concentration in matte. The present results obtained at 1250°C and pSO_2 of 0.25 atm with spinel saturation in slags are close to the observations by Hidayat et al. (2020) and Chen et al. (2019). The increase of temperature and pSO_2 increased the copper concentration in matte at a fixed oxygen partial pressure, when the present results were compared with the data by Hidayat et al. (2016), (2018) and Sineva et al. (2020), Sineva et al. (2021a)). Fallah-Mehrjardi et al. (2018b) investigated the phase equilibria of matte and silica-saturated slag at the same temperature and pSO_2 as in the present study. It can be observed that the copper concentration in matte equilibrated with silica-saturated slag is higher than that equilibrated with spinel saturated slag at the same pO_2 .

3.1.2 Iron in matte vs matte grade

Figure 4(c) shows that the iron concentration in matte decreased from approximately 13 wt% to 2 wt% over the entire matte grade range studied, independent of the corresponding equilibrated type of slag, similar as reported by Sineva et al.

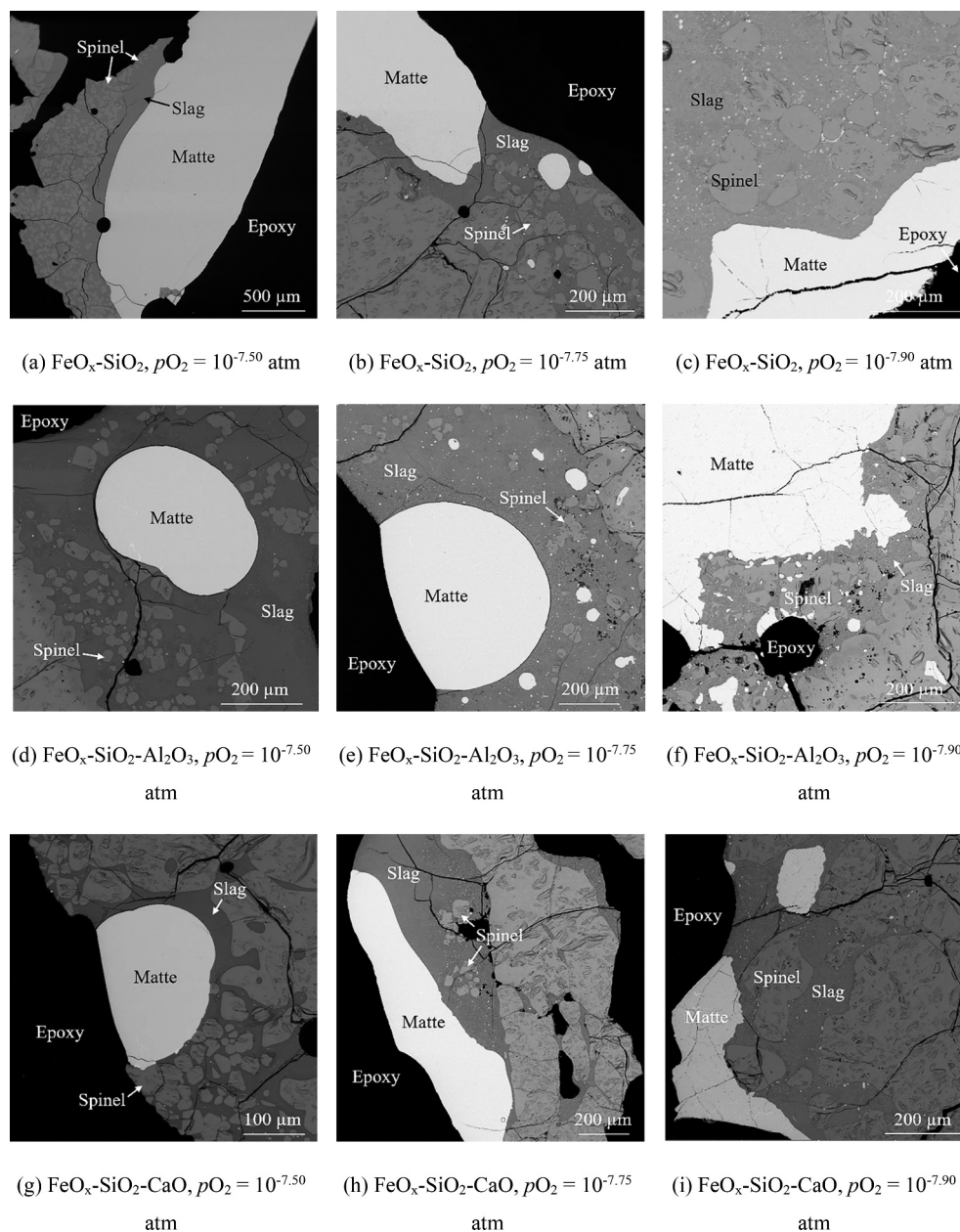


Figure 3. Typical microstructures of matte/slag/spinel equilibrium systems obtained at 1250°C and p_{SO_2} of 0.25 atm; (a)-(c): $\text{FeO}_x\text{-SiO}_2$ slag; (d)-(f): $\text{FeO}_x\text{-SiO}_2\text{-Al}_2\text{O}_3$ slag; (g)-(h): $\text{FeO}_x\text{-SiO}_2\text{-CaO}$ slag.

(2020). The present results are slightly lower than the data from literature (Chen et al. 2019; Fallah-Mehrjardi et al. 2018b; Hidayat et al. 2018; Sineva et al. 2020, 2021a) but displayed similar decreasing trend as a function of matte grade. In the study by Hidayat et al. (2018), (2020), they observed that the increase of temperature from 1200°C to 1250°C, at p_{SO_2} of 0.25 atm had no obvious impact on the iron concentration in matte. Additionally, it was found by Chen et al. (2019), Roghani, Takeda and Itagaki (2000), and Sineva et al. (2021a) that the iron concentration in matte was not affected by the prevailing sulfur partial pressure, like our previous observations for silica-saturated system at 1300°C, $p_{\text{SO}_2} = 0.1\text{--}0.5$ atm.

3.1.3 Sulfur in matte vs matte grade

Figure 4(d) provides the relationship between sulfur concentration in matte and matte grade at 1250°C and p_{SO_2} of 0.25 atm. It can be found that the present sulfur concentration

in matte equilibrated with all types of slags investigated decreased with increasing matte grade, as reported previously (Abdeyazdan et al. 2020a, 2020b; Chen et al. 2019; Fallah-Mehrjardi, Hayes and Jak 2018a; Fallah-Mehrjardi et al. 2017a, 2017b, 2018b; Hidayat et al. 2018, 2016, 2020; Roghani, Takeda and Itagaki 2000; Sineva et al. 2020, 2021a, 2021b). The present results are on the lower side of the data from literature (Chen et al. 2019; Hidayat et al. 2018; Sineva et al. 2020, 2021a), but are still within the range reported previously. Similar to the results of iron in matte, the sulfur concentration in matte were not sensitive to the temperature and prevailing p_{SO_2} of the equilibrium system (Chen et al. 2018; Hidayat et al. 2018; Sineva et al. 2021a). The results by Fallah-Mehrjardi et al. (2018b) obtained at silica-saturation in the matte-slag-gas equilibrium system are close to the data by Hidayat et al. (2018), (2020) determined at spinel saturation of the slag.

Table 3. Experimentally measured compositions of matte, slag, and spinel phases in the matte-slag-spinel-gas equilibrium systems at 1250°C and p_{SO_2} of 0.25 atm.

Slag	Sample	$\text{Log}_{10}[p_{\text{O}_2}, \text{atm}]$	Matte composition/wt%						Liquid slag and solid oxide composition/wt%						Fe/SiO ₂ ratio of slag
			O	Cu	Fe	S	Phase	"FeO"	SiO ₂	Al ₂ O ₃	CaO	Cu	S		
FeO _x -SiO ₂	CSP-14	-7.5	0.66 ± 0.18	75.29 ± 0.41	1.89 ± 0.19	20.44 ± 0.12	Slag	74.33 ± 0.47	23.07 ± 0.52	-	-	-	0.91 ± 0.32	0.24 ± 0.09	2.51 ± 0.06
	CSP-39	-7.5	0.73 ± 0.14	75.04 ± 0.33	1.97 ± 0.14	20.31 ± 0.21	Spinel	99.29 ± 0.01	0.62 ± 0.01	-	-	-	1.06 ± 0.42	0.27 ± 0.11	2.55 ± 0.08
	CSP-15	-7.62	0.75 ± 0.20	72.80 ± 0.42	3.48 ± 0.19	21.09 ± 0.14	Spinel	99.31 ± 0.19	0.60 ± 0.04	-	-	-	1.15 ± 0.44	0.65 ± 0.11	2.88 ± 0.07
	CSP-40	-7.62	0.77 ± 0.09	73.08 ± 0.40	3.41 ± 0.10	20.87 ± 0.14	Spinel	99.29 ± 0.03	0.61 ± 0.02	-	-	-	0.77 ± 0.21	0.60 ± 0.09	2.87 ± 0.12
	CSP-16	-7.75	0.89 ± 0.10	70.08 ± 0.31	5.86 ± 0.13	21.57 ± 0.13	Spinel	99.35 ± 0.02	0.60 ± 0.02	-	-	-	1.15 ± 0.55	1.26 ± 0.19	3.32 ± 0.14
	CSP-41	-7.75	0.95 ± 0.38	69.99 ± 0.77	5.69 ± 0.53	21.40 ± 0.27	Spinel	99.38 ± 0.02	0.58 ± 0.02	-	-	-	0.88 ± 0.17	1.20 ± 0.11	3.22 ± 0.11
	CSP-17	-7.84	1.17 ± 0.15	65.57 ± 0.25	9.17 ± 0.26	22.29 ± 0.10	Spinel	99.27 ± 0.03	0.59 ± 0.02	-	-	-	1.18 ± 0.14	2.47 ± 0.12	4.12 ± 0.11
	CSP-42	-7.84	1.20 ± 0.36	65.56 ± 0.56	9.17 ± 0.40	22.21 ± 0.26	Spinel	80.66 ± 0.48	15.23 ± 0.33	-	-	-	1.28 ± 0.27	2.40 ± 0.21	4.08 ± 0.25
	CSP-18	-7.9	1.76 ± 0.31	60.81 ± 0.64	13.03 ± 0.40	22.58 ± 0.33	Spinel	99.39 ± 0.09	0.54 ± 0.08	-	-	-	1.87 ± 0.38	3.78 ± 0.19	5.48 ± 0.15
	CSP-43	-7.9	1.58 ± 0.29	61.26 ± 0.73	12.70 ± 0.40	22.69 ± 0.42	Spinel	80.44 ± 0.93	15.38 ± 0.80	-	-	-	2.41 ± 0.71	3.89 ± 0.59	5.15 ± 0.50
	CSP-19	-7.5	0.46 ± 0.10	75.65 ± 0.50	1.84 ± 0.13	20.60 ± 0.17	Spinel	99.40 ± 0.02	0.51 ± 0.02	-	-	-	1.24 ± 0.39	0.22 ± 0.09	2.03 ± 0.11
	CSP-34	-7.5	0.74 ± 0.10	75.23 ± 0.40	1.98 ± 0.15	20.54 ± 0.12	Spinel	67.77 ± 1.21	25.94 ± 1.04	4.24 ± 0.41	-	-	1.43 ± 0.43	0.27 ± 0.10	2.16 ± 0.04
	CSP-20	-7.62	0.59 ± 0.20	73.57 ± 0.71	3.10 ± 0.23	20.97 ± 0.16	Spinel	68.90 ± 0.37	24.76 ± 0.40	3.75 ± 0.10	-	-	1.26 ± 0.39	0.43 ± 0.12	2.28 ± 0.09
	CSP-35	-7.62	0.69 ± 0.12	73.15 ± 0.29	3.16 ± 0.14	20.98 ± 0.11	Spinel	92.75 ± 0.81	0.48 ± 0.03	6.74 ± 0.86	-	-	1.23 ± 0.32	0.44 ± 0.07	2.27 ± 0.06
	CSP-21	-7.75	1.01 ± 0.09	70.38 ± 0.26	5.46 ± 0.12	21.45 ± 0.12	Spinel	70.22 ± 0.92	24.02 ± 0.40	3.80 ± 0.37	-	-	0.83 ± 0.30	0.80 ± 0.09	2.64 ± 0.06
	CSP-36	-7.75	0.81 ± 0.25	71.03 ± 0.60	5.14 ± 0.43	21.32 ± 0.31	Spinel	92.85 ± 1.18	0.50 ± 0.03	6.65 ± 1.19	-	-	0.88 ± 0.38	0.82 ± 0.11	2.71 ± 0.09
	CSP-22	-7.84	1.25 ± 0.17	66.79 ± 0.52	8.04 ± 0.23	21.91 ± 0.19	Spinel	73.87 ± 0.72	21.21 ± 0.52	2.78 ± 0.10	-	-	0.64 ± 0.15	1.31 ± 0.09	3.05 ± 0.06
	CSP-37	-7.84	0.97 ± 0.13	67.25 ± 0.31	7.81 ± 0.26	22.00 ± 0.21	Spinel	93.06 ± 0.71	0.52 ± 0.19	6.41 ± 0.79	-	-	0.82 ± 0.26	1.38 ± 0.06	3.09 ± 0.10
CSP-23	-7.9	1.33 ± 0.42	62.92 ± 0.71	10.92 ± 0.55	22.81 ± 0.39	Spinel	75.19 ± 0.59	19.15 ± 0.28	2.53 ± 0.23	-	-	1.33 ± 0.36	2.17 ± 0.21	3.39 ± 0.06	
CSP-38	-7.9	1.39 ± 0.48	63.02 ± 0.84	11.17 ± 0.56	22.62 ± 0.42	Spinel	92.66 ± 1.37	0.49 ± 0.11	6.86 ± 1.41	-	-	0.92 ± 0.23	2.04 ± 0.09	3.43 ± 0.07	
						Spinel	93.37 ± 1.49	0.47 ± 0.04	6.16 ± 1.52	-	-	-	-	-	-
						Spinel	75.83 ± 0.69	17.37 ± 0.30	2.44 ± 0.15	-	-	-	-	-	-
						Spinel	91.46 ± 1.18	0.44 ± 0.03	8.10 ± 1.20	-	-	-	-	-	-
						Spinel	76.89 ± 0.50	17.45 ± 0.32	2.41 ± 0.09	-	-	-	-	-	-
						Spinel	93.79 ± 1.19	0.46 ± 0.05	5.75 ± 1.17	-	-	-	-	-	-

(Continued)

Table 3. (Continued).

Slag	Sample	Log ₁₀ [pO ₂ , atm]	Matte composition/wt%					Liquid slag and solid oxide composition/wt%					Fe/SiO ₂ ratio of slag	
			O	Cu	Fe	S	Phase	"FeO"	SiO ₂	Al ₂ O ₃	CaO	Cu		S
FeO _x -SiO ₂ -CaO	CSP-24	-7.5	0.84 ± 0.13	74.75 ± 0.39	2.05 ± 0.13	20.37 ± 0.11	Slag	63.20 ± 0.33	25.57 ± 0.15	-	6.96 ± 0.03	1.31 ± 0.17	0.28 ± 0.04	1.92 ± 0.02
	CSP-29	-7.5	0.75 ± 0.09	74.76 ± 0.32	1.96 ± 0.07	20.58 ± 0.13	Spinel	99.48 ± 0.04	0.41 ± 0.02	-	7.13 ± 0.04	1.27 ± 0.33	0.28 ± 0.08	1.86 ± 0.01
	CSP-25	-7.62	0.97 ± 0.20	72.90 ± 0.39	3.50 ± 0.23	20.83 ± 0.17	Slag	99.46 ± 0.03	0.43 ± 0.02	-	6.56 ± 0.15	0.73 ± 0.38	0.37 ± 0.10	2.12 ± 0.10
	CSP-30	-7.62	0.83 ± 0.11	72.81 ± 0.29	3.49 ± 0.15	20.89 ± 0.12	Spinel	99.41 ± 0.17	0.46 ± 0.15	-	6.84 ± 0.13	0.71 ± 0.28	0.35 ± 0.07	2.05 ± 0.07
	CSP-26	-7.75	1.22 ± 0.38	69.18 ± 0.63	6.21 ± 0.42	21.46 ± 0.20	Slag	99.50 ± 0.04	0.42 ± 0.02	-	5.89 ± 0.11	0.82 ± 0.24	0.89 ± 0.08	2.43 ± 0.07
	CSP-31	-7.75	1.05 ± 0.10	69.57 ± 0.29	6.02 ± 0.11	21.57 ± 0.12	Spinel	99.49 ± 0.03	0.42 ± 0.02	-	5.95 ± 0.08	1.02 ± 0.32	0.92 ± 0.10	2.40 ± 0.05
	CSP-27	-7.84	1.41 ± 0.20	65.03 ± 0.38	9.36 ± 0.27	22.28 ± 0.19	Slag	99.65 ± 0.21	0.23 ± 0.16	-	4.91 ± 0.08	1.24 ± 0.34	1.71 ± 0.13	3.06 ± 0.09
	CSP-32	-7.84	1.36 ± 0.20	64.63 ± 0.91	9.76 ± 0.63	22.37 ± 0.27	Spinel	99.57 ± 0.10	0.33 ± 0.10	-	4.95 ± 0.05	1.24 ± 0.26	1.74 ± 0.11	3.10 ± 0.03
	CSP-28	-7.9	1.69 ± 0.40	61.02 ± 1.05	12.87 ± 0.60	22.76 ± 0.59	Slag	99.75 ± 0.13	0.15 ± 0.13	-	4.01 ± 0.14	1.37 ± 0.37	2.78 ± 0.28	3.96 ± 0.20
	CSP-33	-7.9	1.83 ± 0.61	60.50 ± 1.22	13.10 ± 0.87	22.69 ± 0.56	Spinel	99.78 ± 0.15	0.10 ± 0.13	-	3.91 ± 0.30	1.31 ± 0.31	2.66 ± 0.29	3.91 ± 0.40

3.1.4 Oxygen in matte vs matte grade

Figure 4(e) displays the dissolved oxygen concentration in matte as a function of matte grade. It was observed that the oxygen in matte decreased along with increasing matte grade, independent of the slag types, fitting well with the findings in previous studies (Chen et al. 2020b, 2020c; Hidayat et al. 2018, 2020; Sineva et al. 2020). It was observed by Hidayat et al. (2018), (2020) that the increase of temperature from 1200°C to 1250°C at pSO₂ of 0.25 atm increased the oxygen concentration in matte and the impact of temperature on oxygen in matte weakened with an increasing matte grade.

3.1.5 Differences between the present study and literature

To demonstrate the reasons for the differences in iron and sulfur concentrations in matte between the present study and previous works (Fallah-Mehrjardi et al. 2018b; Hidayat et al. 2018; Sineva et al. 2020, 2021a), the total concentrations of trace elements (Ag, Ni, Co, and Sn) in matte in this study were calculated and displayed as a function of matte grade, shown in Figure 4(f). It can be seen that the total concentration of trace elements in matte in this study was approximately 1.5–2 wt% and had no significant changes with increasing matte grade. The department of trace elements into the matte phase contributed to the gap between the present study and results from literature (Fallah-Mehrjardi et al. 2018b; Hidayat et al. 2018; Sineva et al. 2020, 2021a). On the other hand, the copper and iron concentrations in matte in the compared studies (Fallah-Mehrjardi et al. 2018b; Hidayat et al. 2018; Sineva et al. 2020, 2021a) were calculated without considering oxygen in matte. They estimated the oxygen concentrations in matte by taking the difference between 100 and the sum of Cu, Fe and S in matte, whereas in the present study, the oxygen concentration in matte was measured and calibrated by obsidian in the EPMA analysis. The different calculation methods for the concentrations of copper, iron, sulfur, and oxygen in matte may also led to the existence of differences between the data.

3.2 Slag composition

3.2.1 Copper in slag vs matte grade

Figure 5(a) shows the copper concentration in slag as a function of matte grade. It can be observed that the copper concentration in all spinel-saturated slags obtained in the present study decreased with increasing matte grade from approximately 60 wt% to 70 wt% Cu, after which it started to increase at higher matte grades, similar to the trends observed by Hidayat et al. (2016), (2018), (2020) and Sridhar, Toguri and Simeonov (1997). However, the copper concentration in the silica-saturated slags increased over the entire matte-grade range (Chen et al. 2020c; Fallah-Mehrjardi et al. 2018b), opposite to the present observations. Hidayat et al. (2018) proposed that the increase of copper in slag at matte grade higher than 70 wt% Cu attributed to the increase of oxidic dissolution of copper in slags, whereas the decreasing trend at lower matte grade was ascribed to the decrease of sulfidic copper dissolution in slag. The concept of sulfidic copper dissolution (Nagamori 1974; Takeda 1992) in slags needs to be furtherly confirmed.

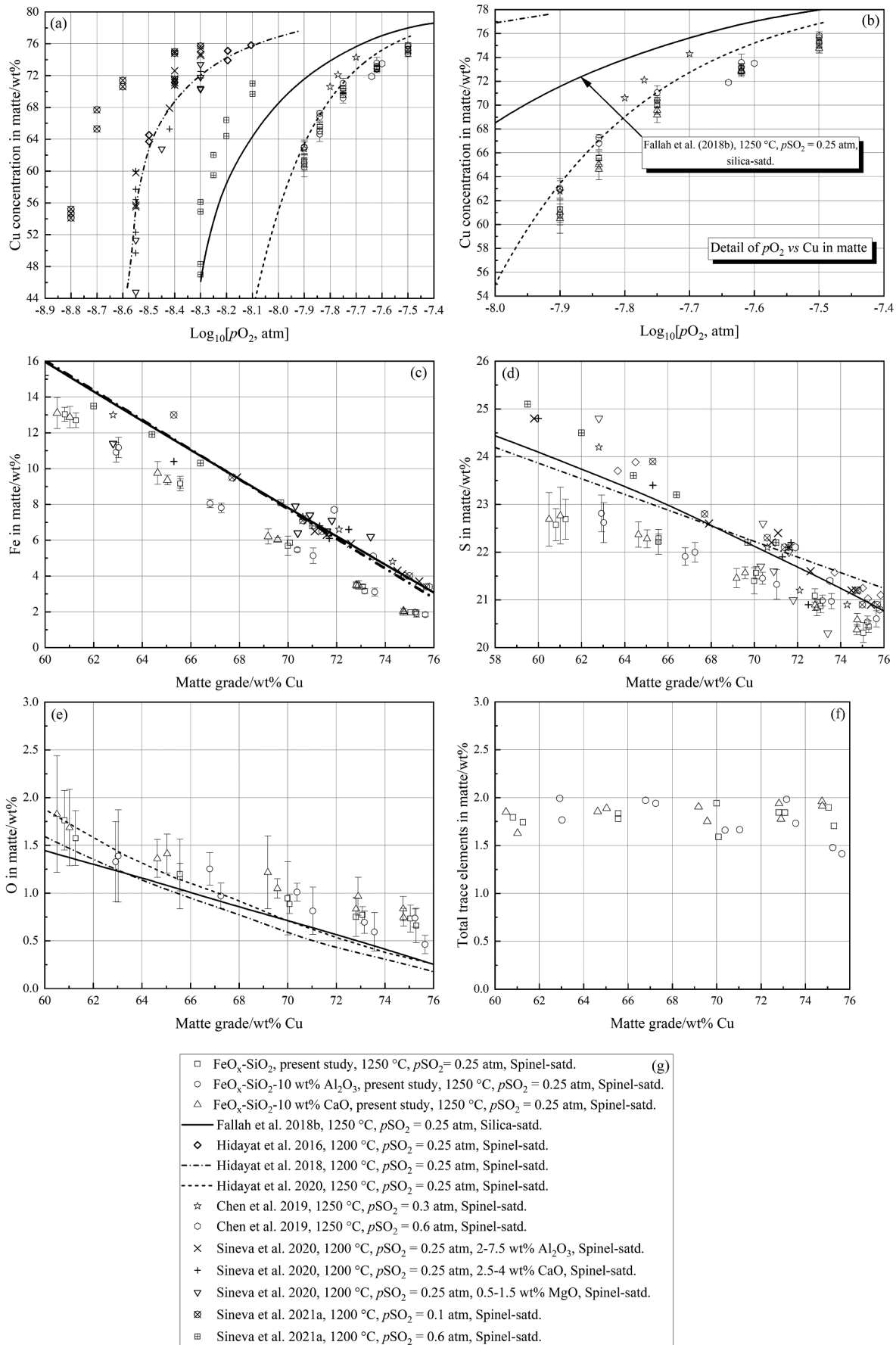


Figure 4. Concentrations of copper (a) and (b), iron (c), sulfur (d), and oxygen (e) in matte vs oxygen partial pressure or matte grade; (f) total concentration of trace elements in matte; (g) markers and legends.

The addition of Al_2O_3 or CaO to the present iron spinel-saturated iron silicate slag decreased the copper concentration in slag at matte grades lower than 70 wt% Cu. However, the copper concentration in the $\text{Al}_2\text{O}_3/\text{CaO}$ -containing slag was higher than that in $\text{FeO}_x\text{-SiO}_2$ slag at higher matte grades. The decreasing impacts of Al_2O_3 , MgO , and CaO were also determined by Sineva et al. (2020) at 1200°C and $p\text{SO}_2 = 0.25$ atm.

Moreover, in another study by Sineva et al. (2021a), they found that an increased prevailing sulfur dioxide partial pressure resulted in a decreased copper solubility in slag at any fixed matte grade. However, in few other studies (Chen et al. 2020c; Roghani, Takeda and Itagaki 2000) the copper solubility in the silica-saturated slag was observed to be independent of the prevailing sulfur dioxide partial pressure. Compared with the

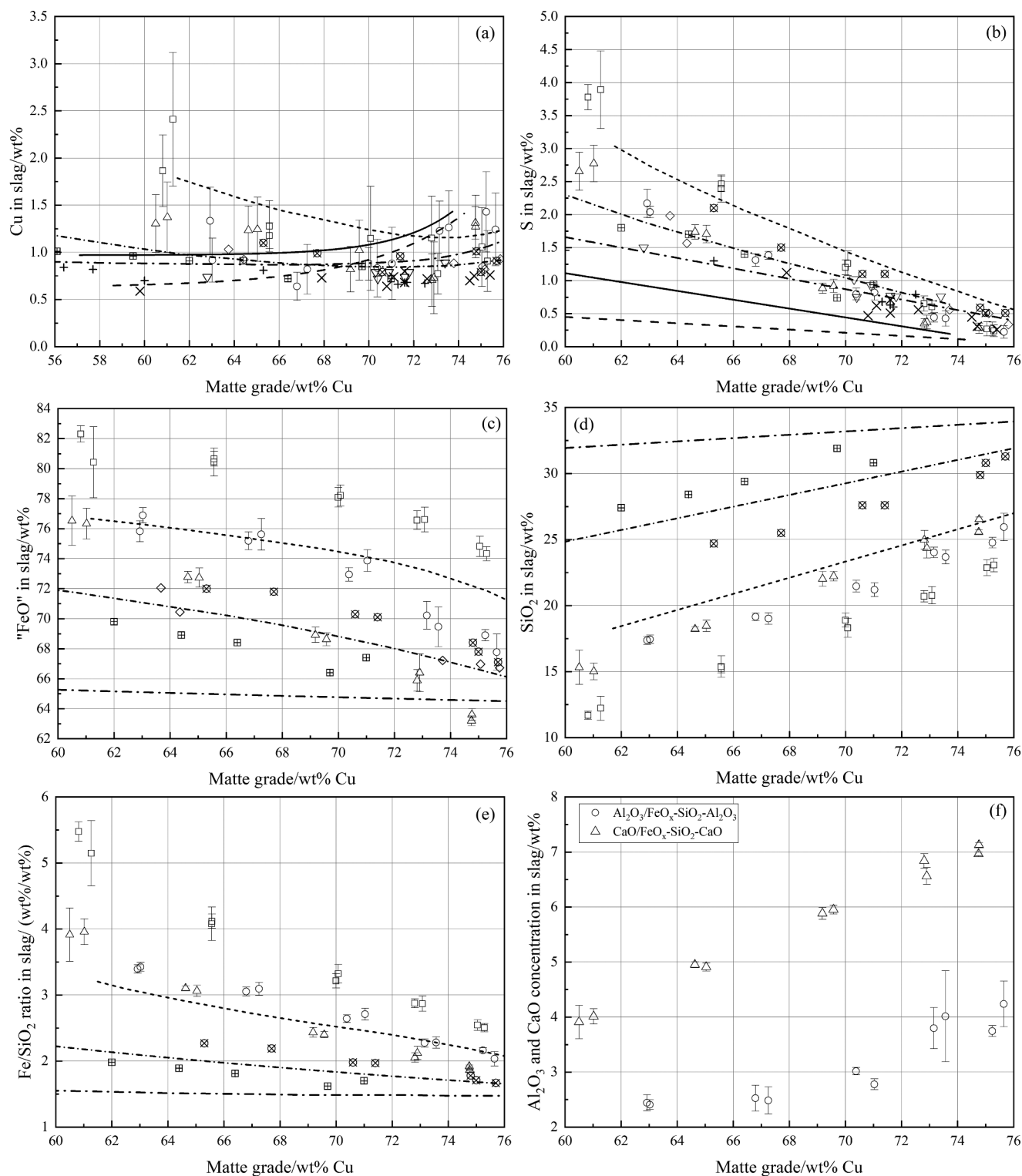


Figure 5. The slag compositions as a function of matte grade or silica concentration in slag; (a) copper; (b) sulfur; (c) "FeO"; (d) silica; (e) Fe/ SiO_2 ratio; (f) alumina and lime in slag; (g) alumina in spinel; (h) distribution coefficient of alumina between spinel and $\text{FeO}_x\text{-SiO}_2\text{-Al}_2\text{O}_3$ slag; (i) markers and legends.

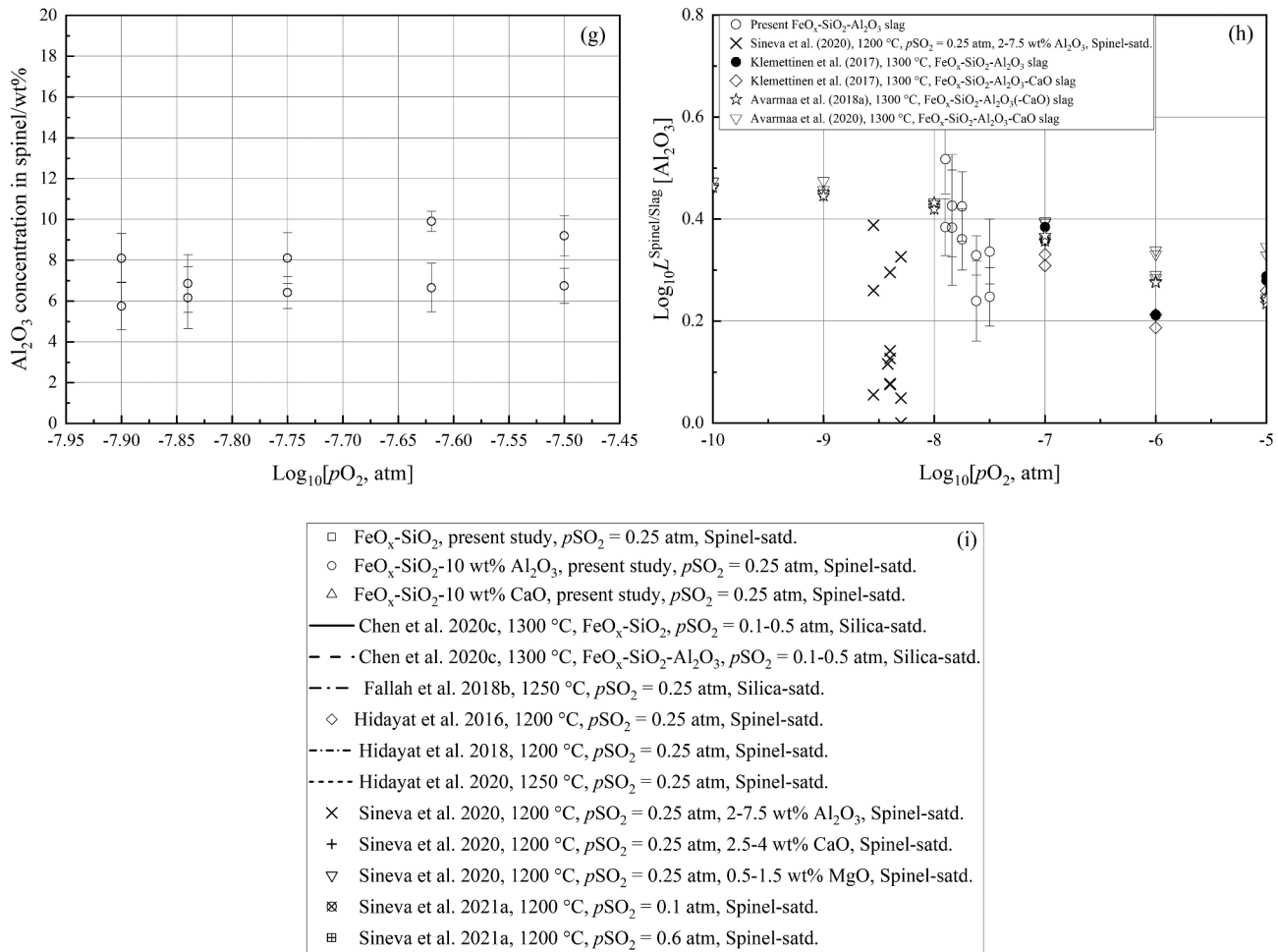


Figure 5. (Continued).

results in previous studies (Hidayat et al. 2018; Sineva et al. 2020, 2021a) obtained at 1200°C and $p\text{SO}_2$ of 0.25 atm, it can be found that the increase of temperature from 1200°C to 1250°C led to an increase of copper concentration in slag.

3.2.2 Sulfur in slag vs matte grade

Figure 5(b) suggests that the sulfur concentration in slags decreased with increasing matte grade, as reported previously (Chen et al. 2020c; Fallah-Mehrjardi et al. 2018b; Hidayat et al. 2018, 2016, 2020; Sineva et al. 2020, 2021a). The present results obtained for FeO_x-SiO₂ slag are close to the observations by Hidayat et al. (2020). The observations from the present alumina/lime-containing slag are similar to the results by Sineva et al. (2020), Sineva et al. (2021a)). In general, the sulfur concentration in the spinel-saturated slag was somewhat higher than that in the silica-saturated slag.

It is evident that the alumina and lime additions effectively decreased the sulfur concentration in slag, fitting well with the observations in the literature (Chen et al. 2020b, 2020c; Fallah-Mehrjardi, Hayes and Jak 2018a; Sineva et al. 2020; Sukhomlinov et al. 2019a). It was observed by Hidayat et al. (2020) that the increase of temperature resulted in a decrease of sulfur dissolution in slag. Sineva et al. (2021a) found that the sulfur concentration in spinel-saturated slag obtained at higher $p\text{SO}_2$ was lower than that obtained at lower $p\text{SO}_2$, whereas in

few other studies (Chen et al. 2020c; Roghani, Takeda and Itagaki 2000), the sulfur content in the silica/MgO-saturated slag was not affected by $p\text{SO}_2$.

3.2.3 "FeO" in slag vs matte grade

It can be seen in Figure 5(c) that the concentration of "FeO" in all spinel-saturated slags in the present study had a similar decreasing trend with increasing matte grade, fitting well with the trends determined by Hidayat et al. (2016), (2018), (2020) and Sineva et al. (2020), Sineva et al. (2021a)). However, the "FeO" concentration in slag at silica-saturation obtained by Fallah-Mehrjardi et al. (2018b) kept almost constant. The increase of oxygen partial pressure resulted in a decrease of iron oxide but an increase of silica content at spinel saturation boundary in the FeO_x-SiO₂ (Chen et al. 2021b), FeO_x-SiO₂-Al₂O₃ (Chen et al. 2020a), and FeO_x-SiO₂-CaO (Yazawa 2000) systems, in contrast, no strong correlation between the prevailing oxygen partial pressure and the silica-saturation boundary was detected in the literature (Fallah-Mehrjardi et al. 2018b).

3.2.4 SiO₂ in slag vs matte grade

Figure 5(d) presents the silica concentration results in the iron spinel-saturated slags. The silica concentration in all slags in the present study increased with increasing matte

grade, as observed in the previous studies (Hidayat et al. 2018, 2020; Sineva et al. 2021a). This is due to the shift of the spinel primary-phase boundary along with pO_2 to the higher silica content region. The increasing trend of silica concentration in the silica-saturated slag (Fallah-Mehrjardi et al. 2018b) was not as significant as that in the spinel-saturated slag, ascribing to the small effect of oxygen partial pressure on the silica primary-phase field, as mentioned beforehand.

3.2.5 Fe/SiO₂ ratio, Al₂O₃, and CaO concentrations in slag vs matte grade

The Fe/SiO₂ ratio as well as the alumina and lime concentrations in the slags are shown in Figure 5(e) and (f), respectively. The Fe/SiO₂ ratio in slags obtained in the present study decreased along with increasing matte grade. This is in a good agreement with the results in previous studies (Hidayat et al. 2018, 2020; Sineva et al. 2021a). The results reported by Fallah-Mehrjardi et al. (2018b), obtained in silica-saturated slags, had no significant changes over the entire matte-grade range studied, which is due to the small changes of “FeO” and silica concentrations in slag at silica saturation. Figure 5(f) shows that the concentrations of alumina and lime in slag increased from approximately 2.5 to 4 wt% and 4 to 7 wt %, respectively, with increasing matte grade. However, the concentration of alumina in slag was lower than that of lime by approximately 3 wt% due to the dissolution of alumina in the spinel phase.

3.2.6 Al₂O₃ in spinel vs Log₁₀[pO₂, atm]

Figure 5(g) indicates that the concentration of alumina in spinel displayed an increasing trend with increasing oxygen partial pressure, ranging from 6 to 10 wt%. The dissolution of alumina in spinel equilibrated with matte and slag was also observed in the study by Sineva et al. (2020). However, the results were quite scattered, and no discussion was presented in their study. Avarmaa, Yliaho and Taskinen (2018a), (2020)) and Klemettinen, Avarmaa and Taskinen (2017) observed that the alumina concentration in the Al-Fe spinel equilibrated with metallic copper and iron silicate slag in alumina crucible were higher than 25 wt% and it had an opposite downward trend with increasing the prevailing oxygen partial pressure of the equilibrium system.

3.2.7 Distribution of Al₂O₃ between spinel and slag

To investigate the distribution behavior of alumina in the matte-slag-spinel-gas equilibrium system, the distribution coefficient of alumina between spinel and slag, $L^{\text{Spinel/Slag}}[Al_2O_3]$, was calculated using the following Eq. (1):

$$\text{Log}_{10} L^{\text{Spinel/Slag}}[Al_2O_3] = \text{Log}_{10} \left(\frac{[\text{wt}\% Al_2O_3]_{\text{in spinel}}}{(\text{wt}\% Al_2O_3)_{\text{in slag}}} \right) \quad (1)$$

where [wt% Al₂O₃] and (wt% Al₂O₃) represent the experimentally measured Al₂O₃ concentration in spinel and slag, respectively. Figure 5(h) shows the logarithmic distribution coefficient of alumina between spinel and slag as a function of logarithmic oxygen partial pressure. It can be found that the logarithmic values were > 0 , indicating that alumina was

preferentially distributed in the spinel phase and its deportment into spinel was promoted with decreasing oxygen partial pressure. Similar decreasing trends were observed by Klemettinen, Avarmaa and Taskinen (2017) and Avarmaa, Yliaho and Taskinen (2018a), (2020)) in the copper-slag equilibrium system. However, the results by Sineva et al. (2020) were scatter without a clear trend against oxygen partial pressure. As the oxidation degree of aluminum is 3+ in slag and spinel, the slope is caused by the variations of the activity coefficients in the phases where alumina is no more a trace substance.

4. Conclusions

The phase equilibria of copper matte and iron spinel-saturated FeO_x-SiO₂, FeO_x-SiO₂-Al₂O₃, and FeO_x-SiO₂-CaO slags were investigated at 1250°C and $pSO_2 = 0.25$ atm in controlled CO-CO₂-SO₂-Ar gas atmospheres using an equilibration-drop-quenching technique. The phase compositions were measured using an electron probe X-ray microanalyzer. Sets of graphs were constructed to describe the compositions of matte and slag as a function of matte grade and oxygen partial pressure. The present experimental results were compared with previous data obtained at silica/spinel saturation in slag.

The comparison of the present results at spinel saturation with previous observations with slags at silica saturation indicates the copper concentration in slags was affected by the primary phase present at the same matte grade. In general, the copper concentration in the spinel-saturated slag was higher than that in the silica-saturated slag at a fixed matte grade, over the matte-grade range lower than 70 wt% Cu. Additionally, an increase of matte grade, i.e. the increase of oxygen partial pressure, had a stronger effect on the spinel primary-phase field than on the tridymite primary-phase domain.

Addition of alumina into spinel-saturated iron silicate slag had a greater impact on the copper concentration in slag when compared with lime addition. This study is useful for improving the copper smelting processes through adjusting the prevailing oxygen partial pressure, temperature as well as by adding fluxes into slags.

Acknowledgments

This study was partly supported by Aalto University, School of Chemical Engineering. Special thanks are given to the Finland's RawMatTERS Finland Infrastructure (RAMI) based at Aalto University, GTK Espoo and VTT Espoo. Min Chen acknowledges the financial support from the China Scholarship Council [number 201806370217] for a PhD grant.

Disclosure statement

No potential conflict of interest was reported by the author(s).

Funding

This work was supported by the China Scholarship Council [201806370217].

ORCID

Min Chen  <http://orcid.org/0000-0003-0544-4359>
 Katri Avarmaa  <http://orcid.org/0000-0002-8632-3788>
 Pekka Taskinen  <http://orcid.org/0000-0002-4054-952X>
 Ari Jokilaakso  <http://orcid.org/0000-0003-0582-7181>

References

- Abdeyazdan, H., A. Fallah-Mehrjardi, T. Hidayat, M. Shevchenko, P. C. Hayes, and E. Jak. 2020a. The effect of MgO on gas-slag-matte-tridymite equilibria in fayalite-based copper smelting slags at 1473 K (1200 °C) and 1573 K (1300 °C), and $P(\text{SO}_2) = 0.25$ atm. *Journal of Phase Equilibria and Diffusion* 41 (1):44–55. doi:10.1007/s11669-020-00778-5.
- Abdeyazdan, H., A. Fallah-Mehrjardi, T. Hidayat, M. Shevchenko, P. C. Hayes, and E. Jak. 2020b. Experimental study of gas-slag-matte-tridymite equilibria in the Cu-Fe-O-S-Si-Al system at 1573 K (1300 °C) and $P(\text{SO}_2) = 0.25$ atm. *Journal of Phase Equilibria and Diffusion* 41 (1):66–78. doi:10.1007/s11669-020-00779-4.
- Avarmaa, K., H. Johto, and P. Taskinen. 2016. Distribution of precious metals (Ag, Au, Pd, Pt, and Rh) between copper matte and iron silicate slag. *Metallurgical and Materials Transactions B* 47 (1):244–55. doi:10.1007/s11663-015-0498-4.
- Avarmaa, K., H. O'Brien, H. Johto, and P. Taskinen. 2015. Equilibrium distribution of precious metals between slag and copper matte at 1250–1350 °C. *Journal of Sustainable Metallurgy* 1 (3):216–28. doi:10.1007/s40831-015-0020-x.
- Avarmaa, K., H. O'Brien, L. Klemettinen, and P. Taskinen. 2020. Precious metal recoveries in secondary copper smelting with high-alumina slags. *Journal of Material Cycles and Waste Management* 22 (3):642–55. doi:10.1007/s10163-019-00955-w.
- Avarmaa, K., H. O'Brien, M. Valkama, L. Klemettinen, E. Niemi, and P. Taskinen. 2018b. Properties of $\text{Na}_2\text{O-SiO}_2$ slags in Doré smelting. *Mineral Processing and Extractive Metallurgy Review* 39 (2):125–35. doi:10.1080/08827508.2017.1391246.
- Avarmaa, K., D. Strengell, H. Johto, P. Latostenmaa, H. O'Brien, and P. Taskinen. 2022. Solubility of chromium in DON smelting. *Mineral Processing and Extractive Metallurgy Review* 43 (2):201–08. doi:10.1080/08827508.2020.1854251.
- Avarmaa, K., S. Yliaho, and P. Taskinen. 2018a. Recoveries of rare elements Ga, Ge, In and Sn from waste electric and electronic equipment through secondary copper smelting. *Waste Management* 71:400–10. doi:10.1016/j.wasman.2017.09.037.
- Chen, M., K. Avarmaa, L. Klemettinen, H. O'Brien, J. Shi, P. Taskinen, D. Lindberg, and A. Jokilaakso. 2021a. Precious metal distributions between copper matte and slag at high PSO_2 in WEEE reprocessing. *Metallurgical and Materials Transactions B* 52B (2):871–82. doi:10.1007/s11663-021-02059-z.
- Chen, M., K. Avarmaa, L. Klemettinen, H. O'Brien, D. Sukhomlinov, J. Shi, P. Taskinen, and A. Jokilaakso. 2020a. Recovery of precious metals (Au, Ag, Pt, and Pd) from urban mining through copper smelting. *Metallurgical and Materials Transactions B* 51B (4):1495–508. doi:10.1007/s11663-020-01861-5.
- Chen, M., K. Avarmaa, L. Klemettinen, J. Shi, P. Taskinen, and A. Jokilaakso. 2020b. Experimental study on the phase equilibrium of copper matte and silica-saturated $\text{FeO}_x\text{-SiO}_2$ -based slags in pyrometallurgical WEEE processing. *Metallurgical and Materials Transactions B* 51B (4):1552–63. doi:10.1007/s11663-020-01874-0.
- Chen, M., K. Avarmaa, L. Klemettinen, J. Shi, P. Taskinen, D. Lindberg, and A. Jokilaakso. 2020c. Equilibrium of copper matte and silica-saturated iron silicate slags at 1300 °C and PSO_2 of 0.5 atm. *Metallurgical and Materials Transactions B* 51B (5):2107–18. doi:10.1007/s11663-020-01933-6.
- Chen, M., K. Avarmaa, P. Taskinen, L. Klemettinen, R. Michallik, H. O'Brien, and A. Jokilaakso. 2021b. Handling trace elements in WEEE recycling through copper smelting—an experimental and thermodynamic study. *Minerals Engineering* 173:107189. doi:10.1016/j.mineng.2021.107189.
- Chen, M., Z. X. Cui, B. J. Zhao, et al. 2015. Slag chemistry of bottom blown copper smelting furnace at Dongying Fangyuan. In *6th International Symposium on High-Temperature Metallurgical Processing*, ed. T. Jiang, 257–64. Cham: Springer. doi:10.1007/978-3-319-48217-0_33.
- Chen, M., Y. Sun, E. Balladares, C. Pizarro, and B. Zhao. 2019. Experimental studies of liquid/spinel/matte/gas equilibria in the Si-Fe-O-Cu-S system at controlled $P(\text{SO}_2)$ 0.3 and 0.6 atm. *Calphad* 66:101642. doi:10.1016/j.calphad.2019.101642.
- Davies, R. H., A. T. Dinsdale, J. A. Gisby, J. A. J. Robinson, and A. M. Martin. 2002. MTDATA-thermodynamic and phase equilibrium software from the national physical laboratory. *Calphad* 26 (2):229–71. doi:10.1016/S0364-5916(02)00036-6.
- Djordjevic, P., N. Mitevka, I. Mihajlovic, D. Nikolic, and Z. Zivkovic. 2014. Effect of the slag basicity on the coefficient of distribution between copper matte and the slag for certain metals. *Mineral Processing and Extractive Metallurgy Review* 35 (3):202–07. doi:10.1080/08827508.2012.738731.
- Fallah-Mehrjardi, A., P. C. Hayes, and E. Jak. 2018a. The effect of CaO on gas/slag/matte/tridymite equilibria in fayalite-based copper smelting slags at 1473 K (1200 °C) and $P(\text{SO}_2) = 0.25$ atm. *Metallurgical and Materials Transactions B* 49B (2):602–09. doi:10.1007/s11663-018-1170-6.
- Fallah-Mehrjardi, A., T. Hidayat, P. C. Hayes, and E. Jak. 2017a. Experimental investigation of gas/slag/matte/tridymite equilibria in the Cu-Fe-O-S-Si system in controlled atmospheres: Development of technique. *Metallurgical and Materials Transactions B* 48B (6):3002–16. doi:10.1007/s11663-017-1073-y.
- Fallah-Mehrjardi, A., T. Hidayat, P. C. Hayes, and E. Jak. 2017b. Experimental investigation of gas/slag/matte/tridymite equilibria in the Cu-Fe-O-S-Si system in controlled gas atmospheres: Experimental results at 1473 K (1200 °C) and $P(\text{SO}_2) = 0.25$ atm. *Metallurgical and Materials Transactions B* 48B (6):3017–26. doi:10.1007/s11663-017-1076-8.
- Fallah-Mehrjardi, A., T. Hidayat, P. C. Hayes, and E. Jak. 2018b. Experimental investigation of gas/slag/matte/tridymite equilibria in the Cu-Fe-O-S-Si system in controlled gas atmosphere: Experimental results at 1523 K (1250 °C) and $P(\text{SO}_2) = 0.25$ atm. *Metallurgical and Materials Transactions B* 49B (4):1732–39. doi:10.1007/s11663-018-1260-5.
- Gisby, J., P. Taskinen, J. Pihlasalo, Z. Li, M. Tyrer, J. Pearce, K. Avarmaa, P. Björklund, H. Davies, M. Korpi, et al. 2017. MTDATA and the prediction of phase equilibria in oxide systems: 30 years of industrial collaboration. *Metallurgical and Materials Transactions B* 48B (1):91–98. doi:10.1007/s11663-016-0811-x.
- Hidayat, T., A. Fallah-Mehrjardi, P. C. Hayes, and E. Jak. 2018. Experimental investigation of gas/slag/ matte/spinel equilibria in the Cu-Fe-O-S-Si system at 1473 K (1200 °C) and $P(\text{SO}_2) = 0.25$ atm. *Metallurgical and Materials Transactions B* 49B (4):1750–65. doi:10.1007/s11663-018-1262-3.
- Hidayat, T., A. F. Mehrjardi, P. C. Hayes, and E. Jak. 2016. Experimental study of gas/slag/matte/spinel equilibria and minor elements partitioning in the Cu-Fe-O-S-Si system. In *Advances in Molten Slags, Fluxes, and Salts: Proceedings of the 10th International Conference on Molten Slags, Fluxes and Salts 2016*, ed. R. G. Reddy, P. Chaubal, P. C. Pistorius, and U. Pal, 1207–20. Cham: Springer. doi:10.1007/978-3-319-48769-4_130.
- Hidayat, T., A. F. Mehrjardi, P. C. Hayes, and E. Jak. 2020. The influence of temperature on the gas/slag/matte/spinel equilibria in the Cu-Fe-O-S-Si system at fixed $P(\text{SO}_2) = 0.25$ atm. *Metallurgical and Materials Transactions B* 51B (3):963–72. doi:10.1007/s11663-020-01807-x.
- Klemettinen, L., K. Avarmaa, and P. Taskinen. 2017. Slag chemistry of high-alumina iron silicate slags at 1300 °C in WEEE smelting. *Journal of Sustainable Metallurgy* 3 (4):772–81. doi:10.1007/s40831-017-0141-5.
- Li, H., and W. J. Rankin. 1994. Thermodynamics and phase relations of the Fe-O-S-SiO₂ (sat) system at 1200 °C and the effect of copper. *Metallurgical and Materials Transactions B* 25B (1):79–89. doi:10.1007/BF02663181.
- Nagamori, M. 1974. Metal loss to slag: Part I. Sulfidic and oxidic dissolution of copper in fayalite slag from low grade matte. *Metallurgical and Materials Transactions B* 5 (3):531–38. doi:10.1007/BF02644646.

- Nikolic, S., P. C. Hayes, and E. Jak. 2009. Liquidus temperatures in the "Cu₂O"-FeO-Fe₂O₃-CaO-SiO₂ system at metallic copper saturation, at fixed oxygen partial pressures, and in equilibrium with spinel or dicalcium ferrite at 1200 °C and 1250 °C. *Metallurgical and Materials Transactions B* 40 (6):910–19. doi:10.1007/s11663-009-9295-2.
- Pouchou, J. L., and F. Pichoir. 1986. Basic expression of "PAP" computation for quantitative EPMA. In *11th International Congress on X-ray Optics and Microanalysis (ICXOM)*, (J. D. Brown and R. H. Packwood, Eds.), Ontario, Canada: Publ. Univ. Western Ontario, pp. 249–256.
- Roghani, G., Y. Takeda, and K. Itagaki. 2000. Phase equilibrium and minor element distribution between FeO_x-SiO₂-MgO-based slag and Cu₂S-FeS matte at 1573 K under high partial pressures of SO₂. *Metallurgical and Materials Transactions B* 31B (4):705–12. doi:10.1007/s11663-000-0109-9.
- Shishin, D., T. Hidayat, S. Decterov, and E. Jak. 2016. Thermodynamic modelling of liquid slag-matte-metal equilibria applied to the simulation of the Peirce-Smith converter. In *Advances in Molten Slags, Fluxes, and Salts: Proceedings of the 10th International Conference on Molten Slags, Fluxes and Salts 2016*, ed. R. G. Reddy, P. Chaubal, P. C. Pistorius, and U. Pal, 1379–88. Cham: Springer. doi:10.1007/978-3-319-48769-4_150.
- Sineva, S., A. Fallah-Mehrjardi, T. Hidayat, P. C. Hayes, and E. Jak. 2020. Experimental study of the individual effects of Al₂O₃, CaO and MgO on gas/slag/matte/spinel equilibria in Cu-Fe-O-S-Si-Al-Ca-Mg system at 1473 K (1200 °C) and p(SO₂) = 0.25 atm. *Journal of Phase Equilibria and Diffusion* 41 (6):859–69. doi:10.1007/s11669-020-00847-9.
- Sineva, S., T. Hidayat, A. Fallah-Mehrjardi, R. Starykh, P. C. Hayes, and E. Jak. 2021a. Experimental investigation of gas-matte-spinel and gas-slag-matte-spinel equilibria in the Cu-Fe-O-S-Si system at 1200 °C: Effect of SO₂ partial pressure. *Mineral Processing and Extractive Metallurgy* 1–8. doi:10.1080/25726641.2021.1919375.
- Sineva, S., M. Shevchenko, P. C. Hayes, and E. Jak. 2021b. Experimental measurements of slag/matte/metal/tridymite phase equilibria in the Cu-Fe-O-S-Si system at 1200 °C. *Mineral Processing and Extractive Metallurgy Review* 1–11. doi:10.1080/08827508.2021.1998042.
- Sridhar, R., J. M. Toguri, and S. Simeonov. 1997. Copper losses and thermodynamic considerations in copper smelting. *Metallurgical and Materials Transactions B* 28 (2):191–200. doi:10.1007/s11663-997-0084-5.
- Sukhomlinov, D., K. Avarmaa, O. Virtanen, P. Taskinen, and A. Jokilaakso. 2019b. Slag-copper equilibria of selected trace elements in black copper smelting. Part I. Properties of the slag and chromium solubility. *Mineral Processing and Extractive Metallurgy Review* 41 (1):32–40. doi:10.1080/08827508.2019.1575212.
- Sukhomlinov, D., K. Avarmaa, O. Virtanen, P. Taskinen, and A. Jokilaakso. 2020. Slag-copper equilibria of selected trace elements in black-copper smelting. Part II. Trace element distributions. *Mineral Processing and Extractive Metallurgy Review* 41 (3):171–77. doi:10.1080/08827508.2019.1634561.
- Sukhomlinov, D., L. Klemettinen, H. O'Brien, P. Taskinen, and A. Jokilaakso. 2019a. Behavior of Ga, In, Sn, and Te in copper matte smelting. *Metallurgical and Materials Transactions B* 50B (6):2723–32. doi:10.1007/s11663-019-01693-y.
- Sun, Y., M. Chen, E. Balladares, C. Pizarro, L. Contreras, and B. Zhao. 2020a. Effect of CaO on the liquid/spinel/matte/gas equilibria in the Si-Fe-O-Cu-S system at controlled P(SO₂) 0.3 and 0.6 atm. *Calphad* 69:101751. doi:10.1016/j.calphad.2020.101751.
- Sun, Y., M. Chen, E. Balladares, C. Pizarro, L. Contreras, and B. Zhao. 2020b. Effect of MgO on the liquid/spinel/matte/gas equilibria in the Si-Fe-Mg-O-Cu-S system at controlled P(SO₂) 0.3 and 0.6 atm. *Calphad* 70:101803. doi:10.1016/j.calphad.2020.101803.
- Sun, Y., M. Chen, Z. Cui, L. Contreras, and B. Zhao. 2020c. Phase equilibrium studies of iron silicate slag under direct to blister copper-making condition. *Metallurgical and Materials Transactions B* 51B (1):1–5. doi:10.1007/s11663-019-01744-4.
- Sun, Y., M. Chen, Z. Cui, L. Contreras, and B. Zhao. 2020d. Phase equilibrium studies of iron silicate slag in the liquid/spinel/white metal/gas system for copper converting process. *Metallurgical and Materials Transactions B* 51B (2):426–32. doi:10.1007/s11663-020-01786-z.
- Sun, Y., M. Chen, Z. Cui, L. Contreras, and B. Zhao. 2020e. Development of ferrous-calcium silicate slag for the direct to blister copper-making process and the equilibria investigation. *Metallurgical and Materials Transactions B* 51B (3):973–84. doi:10.1007/s11663-020-01817-9.
- Sun, Y., M. Chen, Z. Cui, L. Contreras, and B. Zhao. 2020f. Phase equilibria of ferrous-calcium silicate slags in the liquid/spinel/white metal/gas system for the copper converting process. *Metallurgical and Materials Transactions B* 51B (5):2012–20. doi:10.1007/s11663-020-01887-9.
- Sun, Y., M. Chen, Z. Cui, L. Contreras, and B. Zhao. 2020g. Equilibria of iron silicate slags for continuous converting copper-making process based on phase transformations. *Metallurgical and Materials Transactions B* 51B (5):2039–45. doi:10.1007/s11663-020-01901-0.
- Takeda, Y. (1992). Oxidic and sulfidic dissolution of copper in matte smelting slag. In: *Proceedings of the 4th International Conference on Molten Slags and Fluxes*, Sendai, ISIJ, pp. 584–89.
- Wan, X., L. Shen, A. Jokilaakso, H. Eriç, and P. Taskinen. 2021. Experimental approach to matte-slag reactions in the flash smelting process. *Mineral Processing and Extractive Metallurgy Review* 42 (4):231–41. doi:10.1080/08827508.2020.1737801.
- Wang, Q. M., S. S. Wang, M. Tian, D. X. Tang, Q. H. Tian, and X. Y. Guo. 2019. Relationship between copper content of slag and matte in the SKS copper smelting process. *International Journal of Minerals, Metallurgy and Materials* 26 (3):301–08. doi:10.1007/s12613-019-1738-4.
- Yazawa, A. 1974. Thermodynamic considerations of copper smelting. *Canadian Metallurgical Quarterly* 13 (3):443–53. doi:10.1179/cmj.1974.13.3.443.
- Yazawa, A. 2000. Effects of oxygen pressure, Al₂O₃ and MgO on the liquidus surface of FeO_x-SiO₂-CaO system. *Tetsu-to-hagané* 86 (7):431–40. doi:10.2355/tetsuohagane1955.86.7_431.